Effect of Reactive Compatibilisation on the Phase Morphology and Tensile Properties of PA12/PP Blends

S. Jose,[1] S. V. Nair,[1] S. Thomas,[1] J. Karger-Kocsis[2]

[1]*School of Chemical Sciences, Mahatma Gandhi University, Priyadarshini Hills P.O., Kottayam, Kerala, India-686 560*
[2]*Institute for Composite Materials, Kaiserslautern University of Technology, Kaiserslautern, Germany*

Received 20 January 2004; accepted 31 January 2005
DOI 10.1002/app.22806
Published online 19 December 2005 in Wiley InterScience (www.interscience.wiley.com).

ABSTRACT: Both uncompatibilized and compatibilized blends based on polyamide 12 (PA12) and isotactic polypropylene (PP) were prepared in a Brabender Plastograph®. The compatibiliser used was maleic anhydride functionalized polypropylene (PP-g-MA). Phase morphology of the blends was inspected in scanning electron microscope (SEM) on cryogenically fractured etched surfaces of the specimens. PA12/PP blends possessed a nonuniform and unstable morphology owing to the incompatibility between their constituents. Addition of compatibiliser improved the interfacial characteristics of the blends by retarding the rate of coalescence. So, the phase morphology became more fine, uniform, and stable. Tensile properties of both uncompatibilized and compatibilized blends were measured as a function of blend composition and compatibiliser concentration. Uncompatibilized blends displayed inferior mechanical properties to compatibilized ones; especially for those containing 40–60 wt % of PP. Reactive compatibilisation of blends was found to be efficient and improved the tensile strength of the blends considerably. Addition of PP-g-MA improved the interfacial adhesion, decreased the interfacial tension, and thereby, enhanced the tensile strength by 85%. Finally, various models were adopted to describe the tensile strength of the blends. The experimental data exhibited a reasonably good fit with Nielsen's first power law model. J Appl Polym Sci 99: 2640–2660, 2006

Key words: blends; tensile properties; miscibility; morphology; reactive processing

INTRODUCTION

Polyamide 12 (PA12) belongs to the family of engineering thermoplastic showing excellent mechanical and thermal properties. It is the least water absorbing polyamide. Isotactic polypropylene (PP) is one of the cheapest and lightest commodity thermoplastics, with good strength and solvent resistance but poor impact properties. Blending, which is a simple and efficient method to combine the superior properties of these two polymers, would lead to a new polymeric material having good mechanical and thermal properties coupled with excellent solvent resistance. However, the performance of polymer blends depends not only on the nature and composition of the components, but also on the phase morphology and interface characteristics. Unfavorable molecular or segmental level interactions between the components at the interface owing to high interfacial tension result in poor interfacial adhesion between the phases. This leads to an unstable morphology with inferior mechanical properties.

Correspondence to: S Thomas (sabut552001@yahoo.com), (sabut@sancharnet.in).

Journal of Applied Polymer Science, Vol. 99, 2640–2660 (2006)

Compatibilisation of immiscible polymer blends through the regulation of interfacial properties and stabilization of phase morphology against coalescence is the most general and efficient strategy to convert poor multiphase blend systems into high performance alloys. Morphology generation in multiphase systems involves a competition between break-up and coalescence of the minor phase. Thus, the main challenge of the compatibiliser is to minimize the rate of coalescence and to generate a stable and optimum morphology with maximum product performance.

Several researchers have extensively reviewed the role of compatibilisers in multiphase blend systems.[1–5] It has been reported that compatibiliser locates at the interface and suppresses coalescence by stabilizing the interface.[6] Compatibilisation is generally accomplished by adding presynthesized copolymers[7–12] or through reactive processing. In the former case, it is important that the copolymer stays at the interface, without dissolving in either of the two polymers or forming mesophase of micelle structure. The principle role of premade block copolymers in controlling morphology appears to be in preventing coalescence.[7] Lee et al.[8] have investigated the compatibilising performance of random copolymer in the melt state and found that the copolymer forms an encapsulating layer at the interface between the polymers during melt mixing. However, this encapsulating layer did

not provide stability against static coalescence. Mekhilef et al.[9] have shown that addition of copolymer reduced the interfacial tension and, thereby, stabilized the morphology. Oshishi et al.[11] studied the phase morphology and mechanical properties of polymer blends the in presence of a block copolymer as compatibiliser and found that the copolymer successfully compatibilized the blends. It has been suggested that the compatibilising efficiency of block copolymer is influenced by several factors such as chemical composition, number of blocks, and the related molecular characteristics.[10] Harrats et al.[12] reported that tapered block copolymer is the most efficient emulsifier among different block copolymers.

Reactive compatibilisation is a rapid and heterogeneous reaction that takes place across the phase boundary, and in that case, the compatibiliser is generated in situ (i.e., during blending) through grafting or exchange reactions. Effect of reactive compatibilisation on the morphology,[13–20] mechanical,[21–26] crystallization,[27] rheological,[28–30] dynamic mechanical,[31] and barrier[32,33] properties were reported extensively in literature. George et al.[13] have reported that maleic anhydride (MA) containing compatibiliser improved the 'interfacial condition' and, thereby, reduced the dispersed phase size and provided more uniform particle size distribution. Sathe and coworkers[21] studied the effect of concentration of polypropylene (PP) grafted with butyl acrylate compatibiliser on the thermal, morphological, and mechanical properties of PP/PA6 blends and observed that compatibilized blends exhibited superior properties. Marco et al.[27] have reported that presence of a compatibilising agent leads to a decrease in the crystallinity of the polyamide and in its rate of crystallization in PA/PP blends, because of the diluent effect of the molten PP. George et al.[30] have reported on the effect of reactive compatibilisation on the morphology and rheological behavior of thermoplastic elastomers derived from polyethylene/nitrile rubber blends and observed that compatibilisers (a) decreased interfacial tension values, (b) increased the blend viscosity, and (c) made narrow the particle distribution curves.

A particularly interesting feature of polyamides for reactive coupling to other polymers is their inherent chemical functionality, i.e., amine or carboxyl groups and even the amide (peptide) linkage itself. MA-containing interfacial agents can improve the compatibility of the blends through interfacial chemical reactions. The mechanism of the interfacial chemical reaction is based on (a) the amine-anhydride reaction that involves an acid/amide intermediate which cyclices to produce an imide group and a water molecule [Fig. 1(a)], or (b) an amide-anhydride mechanism that involves an acid/imide intermediate which cyclices, leading to a cyclic imide and an acid chain end [Fig. 1(b)].[34]

The important objective of the present study is to monitor the effect of compatibiliser on the phase morphology and mechanical properties of PA12/PP blends. Both compatibilized and uncompatibilized blends were prepared. PP-g-MA was used as compatibiliser. Phase morphology of the blends was evaluated from SEM micrographs. Mechanical properties of the blends were determined as a function of blend ratio and compatibiliser concentration. Attempts were made to correlate the phase morphology changes in presence and absence of compatibiliser with mechanical properties. Finally, various theoretical models were applied to evaluate and compare the experimental values of tensile strength.

EXPERIMENTAL

Materials

Isotactic polypropylene (Koylene 3060) having a melt flow index (MFI) of 3 dg/min (at 230°C/2.16 kg) and a density of 0.90 g/cm^3 was kindly supplied by Indian Petro Chemicals Limited, Baroda, Gujarat, India. PA12, (Vestamid, L1670) having a melt volume-flow rate (MVR) of 60 cm^3/10 min (at 250°C/2.16 kg) and a density of 1.01 g/cm^3 was kindly supplied by Degussa, High Performance Polymers, Marl, Germany.

PP-g-MA (Polybond 3200) having MFI 110 dg/min and MA content 1.0 wt % was obtained by the courtesy of Crompton Corp., Middlebury.

Preparation of uncompatibilized and compatibilized PA12/iPP blends

Both uncompatibilized and compatibilized blends were prepared by melt mixing process in a Brabender Plastograph®. Appropriate amounts of PA12 and PP were mixed at 185°C and 60 rpm for 6 min to obtain blends of different compositions (PA12/PP = 90/10, 80/20, 70/30, 60/40, 50/50, 40/60, 30/70, 20/80, and 10/90). These blends are represented as N_{90}, N_{80} and so on, where subscripts represent the wt % of PA12. Blend containing 30 wt % of PP (N_{70}) was selected for compatibilisation. The compositions of the compatibilized blends are represented in Table I. Compatibilized blends were obtained in two-step mixing process. In the first step the compatibiliser was premixed with PP for 2 min at 185°C and 60 rpm and in the second step PA12 was added to this mixture and mixing was continued for further 5 min. The amount of compatibiliser was varied from 1 to 10 wt % to determine the optimum compatibiliser concentration. Both uncompatibilized and compatibilized blends were compression molded to obtain sheets of 2 mm thickness for mechanical testing.

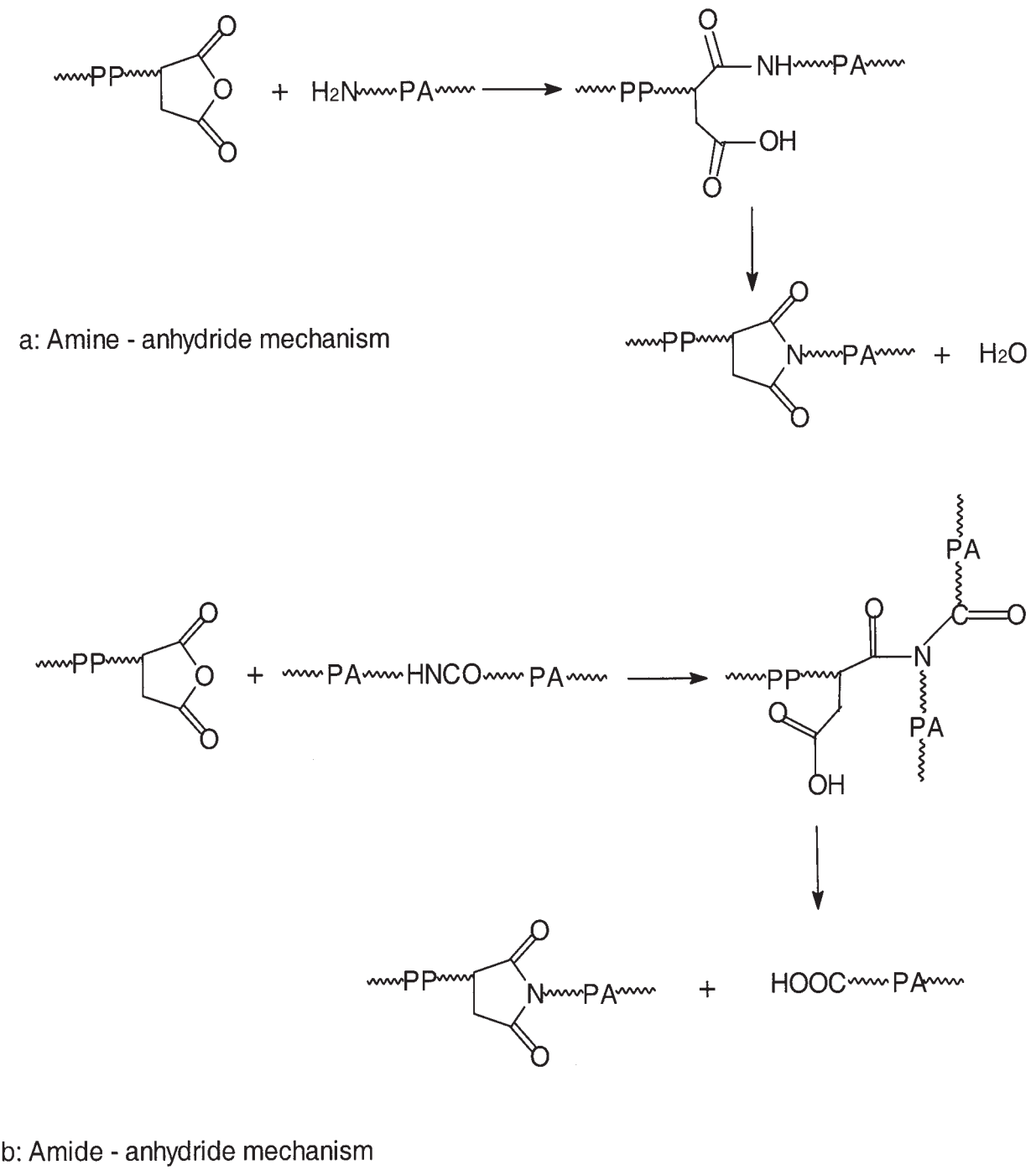

Figure 1 (a) Amine–anhride mechanism.(b) Amide–anhyciride mechanism.

Phase morphology of blends

The specimens for phase morphology studies were cryogenically fractured in liquid nitrogen. The fractured surface was etched in formic acid at ambient temperature for 48 h and in boiling xylene for 72 h to extract the PA12 and PP phases, respectively. The etched surface was sputter coated by gold for 150 s. A minimum of five photographs were taken for each sample, using a scanning electron microscope (SEM; Jeol 5400, Tokyo, Japan).

TABLE I
PA12/PP Compatibilized Blends

Designation	Composition		
	PA12	PP	PP-g-MA
C_1	70	29	1
C_3	70	27	3
C_5	70	25	5
C_{10}	70	20	10

About 400 particles were considered to determine the droplet diameter of the dispersed phase. The number (D_n), weight (D_w), and volume (D_v) average diameters were determined using the following equations; The number average diameter

$$D_n = \frac{\Sigma NiDi}{\Sigma Ni} \quad (1)$$

The weight average diameter

$$D_w = \frac{\Sigma NiDi^2}{\Sigma NiDi} \quad (2)$$

The volume average diameter

$$D_v = \frac{\Sigma NiDi^3}{\Sigma NiDi^2} \quad (3)$$

Mechanical properties of blends

Tensile specimens were punched out from the compression-molded sheets. Tensile tests were performed in accordance with ASTM D412–80 test method using dumb-bell shaped test pieces at a crosshead speed of 50 mm/min, using a Zwick universal testing machine (Ulm, Germany).

RESULTS AND DISCUSSION

Phase morphology of blends

It is unequivocally established that the ultimate properties of polymer blends are influenced by the morphology (i.e., the size, shape, and distribution of the phases in the blends) and the phase interaction. The final blend morphology is determined by factors related to the material parameters (blend composition, viscosity ratio, elasticity ratio, and interfacial tension) and processing conditions[35–40] (temperature, residence time and intensity of mixing, and nature of flow). Based on these facts, several investigations were undertaken to develop empirical rules for the prediction of the phase structure in immiscible blends. However, no reliable theory or empirical rule explaining the dependence of phase structure on these parameters of a system has been derived so far.

The relative importance of the applied viscous forces and the interfacial forces can be expressed in terms of a dimensionless number called capillary number, which is given as:

$$Ca = \frac{\eta_m \dot{\gamma} R}{\tau} \quad (4)$$

where η_m is the viscosity of the matrix, γ is the shear rate, R is the droplet radius and τ is the interfacial tension.

When the Ca exceeds a critical value, the droplet will deform and subsequently break up under the influence of the interfacial tension. However, one should note that the critical Ca value (Ca_{crit}) for break up of the droplet strongly depends on the viscosity ratio, P ($P = \eta_{dispersed}/\eta_{matrix}$ measured under identical conditions). The pioneering work to propose a relationship between Ca and P has been done by Taylor[41] who derived an expression for the Ca_{crit} in the simple shear flow from a Newtonian fluid as:

$$Ca_{crit} = \frac{1}{2}\left(\frac{16P + 16}{19P + 16}\right) \quad (5)$$

Using, $Ca = Ca_{crit}$, one can calculate the droplet diameter D as:

$$D = \frac{2Ca_{crit}\tau}{\dot{\gamma}\eta_m} \quad (6)$$

However, Wu[42] demonstrated that for extruded polymer blends, this equation may be modified as:

$$D = \frac{4\tau P^{\pm 0.84}}{\dot{\gamma}\eta_m} \quad (7)$$

The exponent is positive for $P > 1$ and negative for $P < 1$. The elastic contribution to the effective interfacial tension under dynamic conditions has been estimated from the relation proposed by Van Oene,[43]

$$\alpha_{eff} = \alpha + \frac{d}{12}[(N_2)_d - (N_2)_m] \quad (8)$$

where α_{eff} is the effective interfacial tension under dynamic conditions, α is the static interfacial tension, d is the droplet diameter, $(N_2)_d$ and $(N_2)_m$ are the second normal stress functions for the dispersed phase and for the matrix, respectively.

The phase morphology of cryogenically fractured, etched surfaces of uncompatibilized PA12/PP blends can be evaluated making use of the SEM micrographs presented in Figure 2. All the micrographs clearly reveal two-phase morphology of typical uncompatibilized blends. Two types of morphologies can be distinguished for the blends from the figure: (a) particle-droplet type morphology in blends with 10–40 wt % PP and with 10–30 wt % of PA12 [Fig. 2(a–c) and Fig. 2 (e,f), respectively], and (b) cocontinuous morphology in blends with 50 to 60 wt % PP [Fig. 2(d)].

Table II presents the morphological parameters derived from SEM analysis of cryogenically fractured

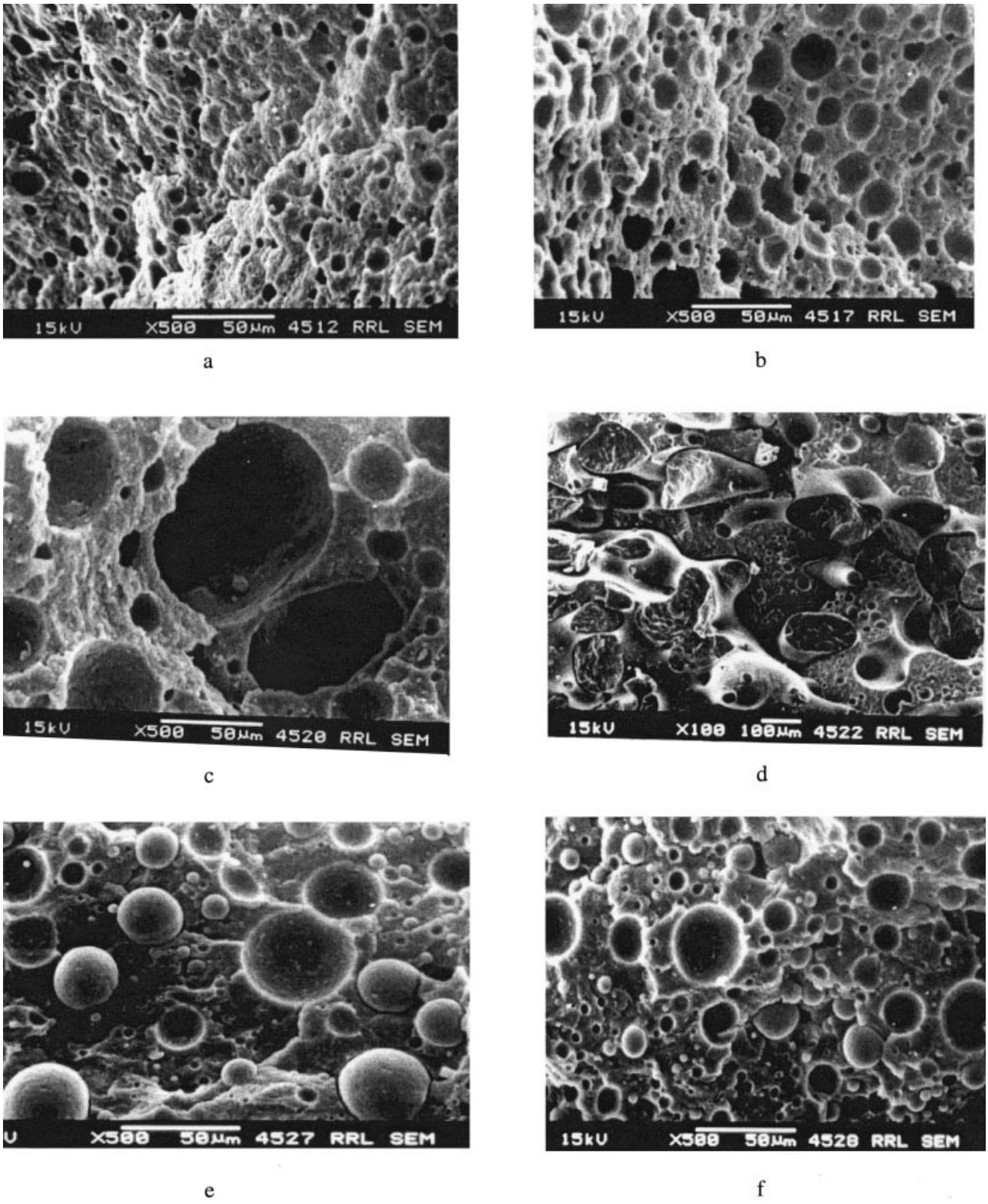

Figure 2 Scanning electron micrographs of PA12/PP suncompatibilised blends.

etched surfaces of the blends. It is evident from this table and Figure 3, which present the variation of average domain size as a function of blend composition, that the average domain size of the dispersed PP phase increases monotonically up to 40 wt % of PP concentration. This is clearly due to coalescence pro-

TABLE II
Morphological Parameters of PA12/PP Uncompatibilized Blends from SEM Analysis

Designation	Composition of PA12/PP	D_n (μm)	D_w (μm)	D_v (μm)	D_w/D_n	A_i (μm)^2/(μm)^3	IPDC (μm)
N_{90}	90/10	7.4	7.8	8.2	1.05	0.08	5.44
N_{80}	80/20	11.1	13.9	14.9	1.25	0.11	4.20
N_{70}	70/30	13.9	16.4	16.8	1.18	0.13	2.82
N_{60}	60/40	38.0	46.0	54.1	1.21	0.06	3.56
N_{30}	30/70	21.0	27.4	31.9	1.30	0.09	4.27
N_{20}	20/80	8.5	12.9	13.5	1.59	0.14	3.20
N_{10}	10/90	5.0	5.3	5.7	1.05	0.12	3.68

cess that may arise from several types of interactions such as:

1. van der Waals forces between neighboring particles
2. capillary forces
3. buoyancy resulting from the different gravities of the two components
4. friction resulting from viscous flow.

Blends with dispersed PA phase in continuous PP matrix also show similar behavior due to the same reason. This behavior can be explained by considering Tokita's equation[44] which explains the dependence of concentration of the dispersed phase on the coalescence rate.

$$d_e \cong 24\ P_r\sigma/\pi\tau_{12}\{\phi_d + (4\ P_rE_{\mathrm{dk}}/\pi\tau_{12})\phi_d^2\} \qquad (9)$$

where d_e is the particle size at equilibrium, τ_{12} is the shear stress, σ is the interfacial tension, E_{dk} is the bulk breaking energy, ϕ_d is the volume fraction of the dispersed phase and P_r is the probability that a collision to resulting coalescence. From this equation it is clear that as the volume fraction of the dispersed phase increases, d_e increases.

It should be noted that for a given dispersed phase concentration, PA particles are smaller than corresponding PP particles. The plausible explanation for this observation mainly depends on the viscosity ratio of the components in the blend. When the lower viscosity component forms the dispersed phase, because of the restricted diffusion of the dispersed particles in more viscous medium, rate of coalescence decreases. The critical coalescence time t_c is given as:

$$t_c = (3\eta_m R/2\sigma)\ \ln(R/2h_c) \qquad (10)$$

where η_m is the matrix viscosity, R is the radius of particle, and h_c is the critical separation distance between the particles. However, it is interesting to note that size of dispersed PP particles in N_{70} blends is smaller than corresponding PA particles in N_{30} blend. An explanation for this contradictory observation may be given on the basis of less unfavorable interaction between the PP domains or relatively high van der Waals forces between PA particles at high concentration.

The distribution of dispersed particles in continuous matrix can be evaluated from the polydispersity, D_w/D_n, presented in Table II. It is seen that for low concentration of the dispersed phase (10 wt %), the distribution of particles is narrow for both PP and PA dispersed phases. However, N_{20} blend shows the broadest particle distribution. For all other blends, the particle distribution was found to be intermediate.

The interfacial area per unit volume has been estimated using the relationship;

$$A_i = 3\phi/R \qquad (11)$$

where ϕ is the volume fraction of the dispersed phase and R is the average radius of dispersed particles in a given blend. The values are presented in Table II. It has been observed that the interfacial area increases as the wt % of dispersed PP phase in the PA matrix increases. However, one can see that interfacial area has lower value for N_{60} and N_{70} blends. It is also obvious from Table II that interfacial area increased marginally as the concentration of PA increased from 10 to 20 wt %. However, N_{30} has lower value than N_{20}. It should be noted that the drop in interfacial area is observed for those compositions (N_{60} and N_{30}) that show maximum increase in domain size. Since interfacial area is a measure of interfacial thickness, which in turn is a measure of compatibility of the blends, all the blends, especially N_{60} and N_{30}, are highly incompatible and are characterized by very narrow interface, which may fail to transfer stress between the phases.

The critical inter particle distance (IPDC) has been calculated from Wu's equation[45]:

$$\mathrm{IPDC} = D[(\pi/6\phi) - 1]^{1/3} \qquad (12)$$

where D is the average domain diameter of the dispersed phase of volume fraction ϕ. High values of IPDC indicate brittle behavior of the blends. The IPDC

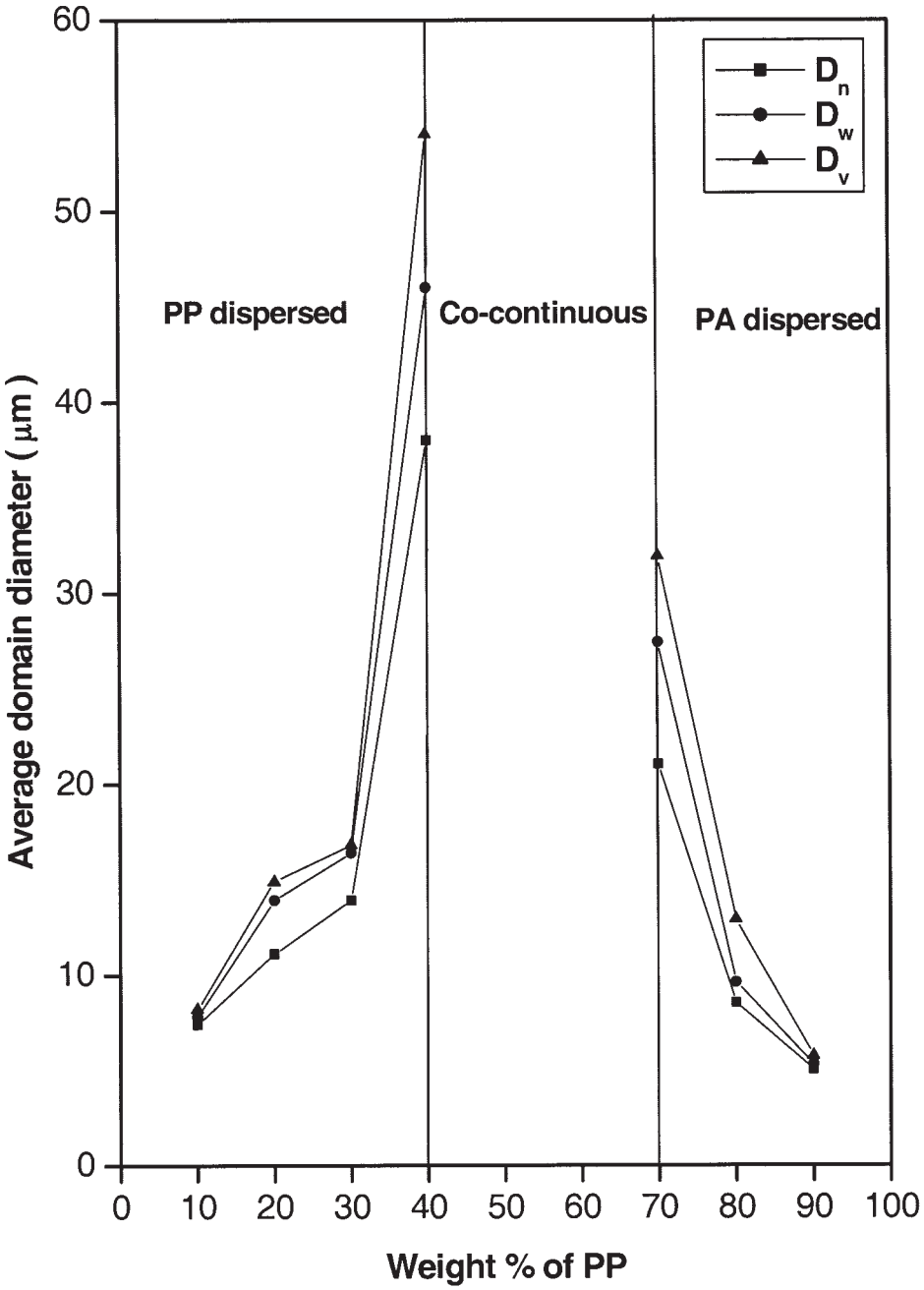

Figure 3 Variation of average domain size of dispersed phase in PA12/PP blends as a function of wt % of PP.

decreases as the concentration of dispersed PP phase increases, reaches a minimum value at 30 wt % of PP, and increases beyond that. Similarly, the IPDC of PA dispersed particles decreased first (from N_{10} to N_{20}) and thereafter increased. N_{70} possessed maximum value of IPDC. Based on the relatively high values of IPDC, one can claim that all the blends will break in a brittle manner. The morphological parameters of N_{50} and N_{40} blends have not been estimated since these blends exhibited typical cocontinuous morphology.

The phase morphology of cryogenically fractured surfaces of 70/30 compatibilized blends has been evaluated from SEM micrographs presented in Figure 4. Table III summarizes the morphological parameters of PA12/PP 70/30 (N_{70}) compatibilized blends. From this table as well as from Figure 5, which demonstrates the variation of average domain diameter as a function of compatibiliser concentration, one can see that the average particle size decreases in presence of compatibiliser. Attention should be paid to the fact that beyond 5 wt % addition of the compatibiliser, there is no appreciable decrease in particle size. This is an indication of the fact that 5 wt % compatibiliser is sufficient to saturate the interface. The reduction in particle size

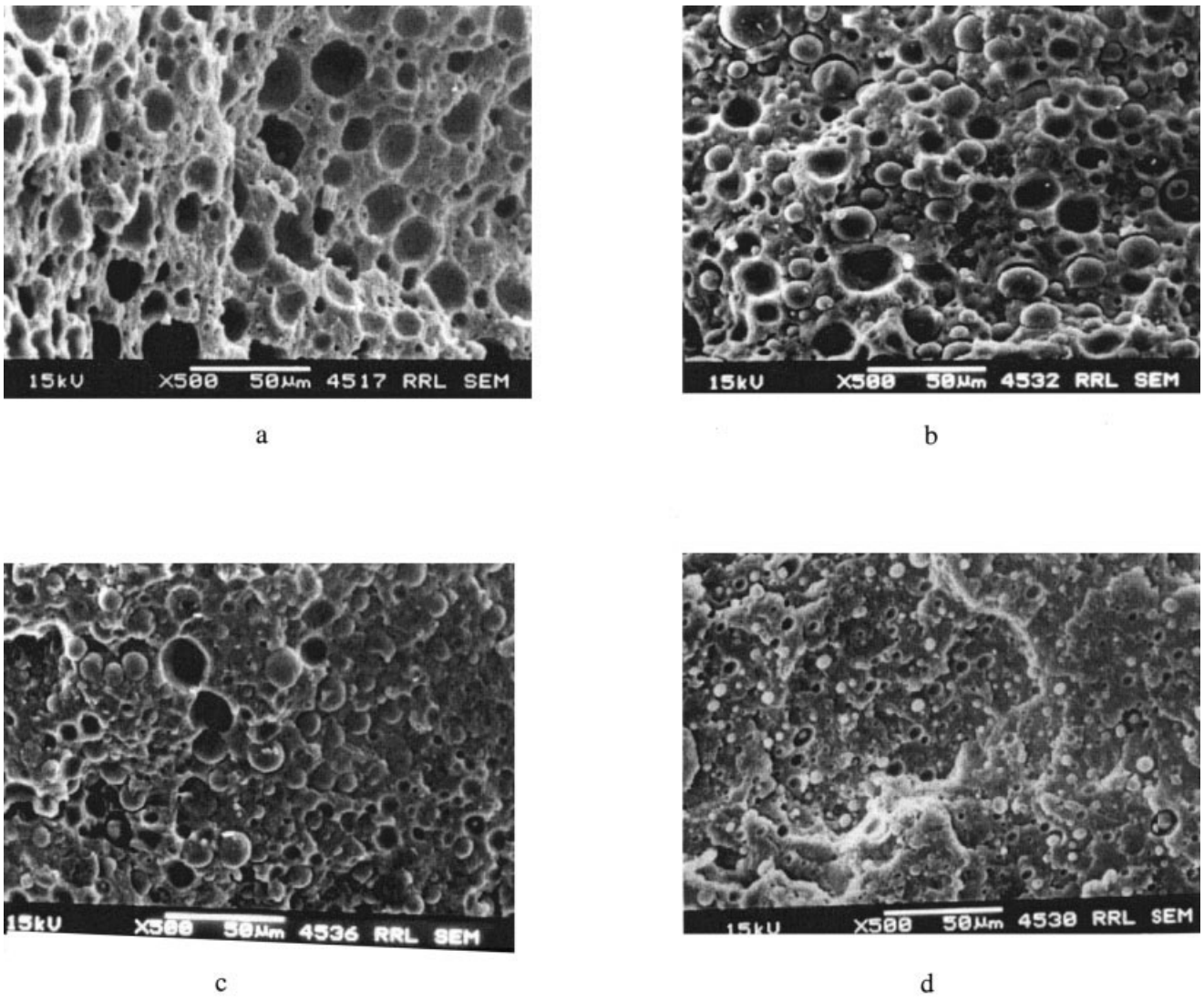

Figure 4 Effect of compatibilisation on the phase morphology of PA12/PP 70/30 blends.

is due to the decrease in the rate of coalescence in presence of compatibiliser. Lepers et al.[14] investigated the relative role of coalescence and interfacial tension in controlling the dispersed phase size reduction during compatibilisation of polyethylene terephthalate/PP (PET/PP) blends. They observed a direct relationship between the drop in the interfacial tension and the dispersed phase reduction of the blend in the presence of interfacial modifier.

It has been established that one can divide coalescence process into four stages as follows[46]:

The first step is the approach of particles with radii R_1 and R_2 and formation of the parallel films between the particles with thickness h_0.

$$h_0 = 9C^2R_{\min}/8\lambda^2[\{6\lambda^2(\lambda + 1)/9C^2(3\lambda + 2)\}^{1/2} - 1]^2 \quad (13)$$

TABLE III
Morphological Parameters of PA12/PP 70/30 Compatibilized Blend (N_{70}) from SEM Analysis

Designation	D_n (μm)	D_w (μm)	D_v (μm)	D_w/D_n	A_i (μm)^2/(μm)^3	IPDC (μm)
N_{70}	13.9	16.4	16.8	1.18	0.130	2.82
C_1	13.2	14.5	14.9	1.10	0.138	2.68
C_3	12.5	13.5	12.6	1.08	0.144	2.54
C_5	9.4	10.1	11.4	1.07	0.192	1.91
C_{10}	9.2	9.7	10.7	1.05	0.196	1.87

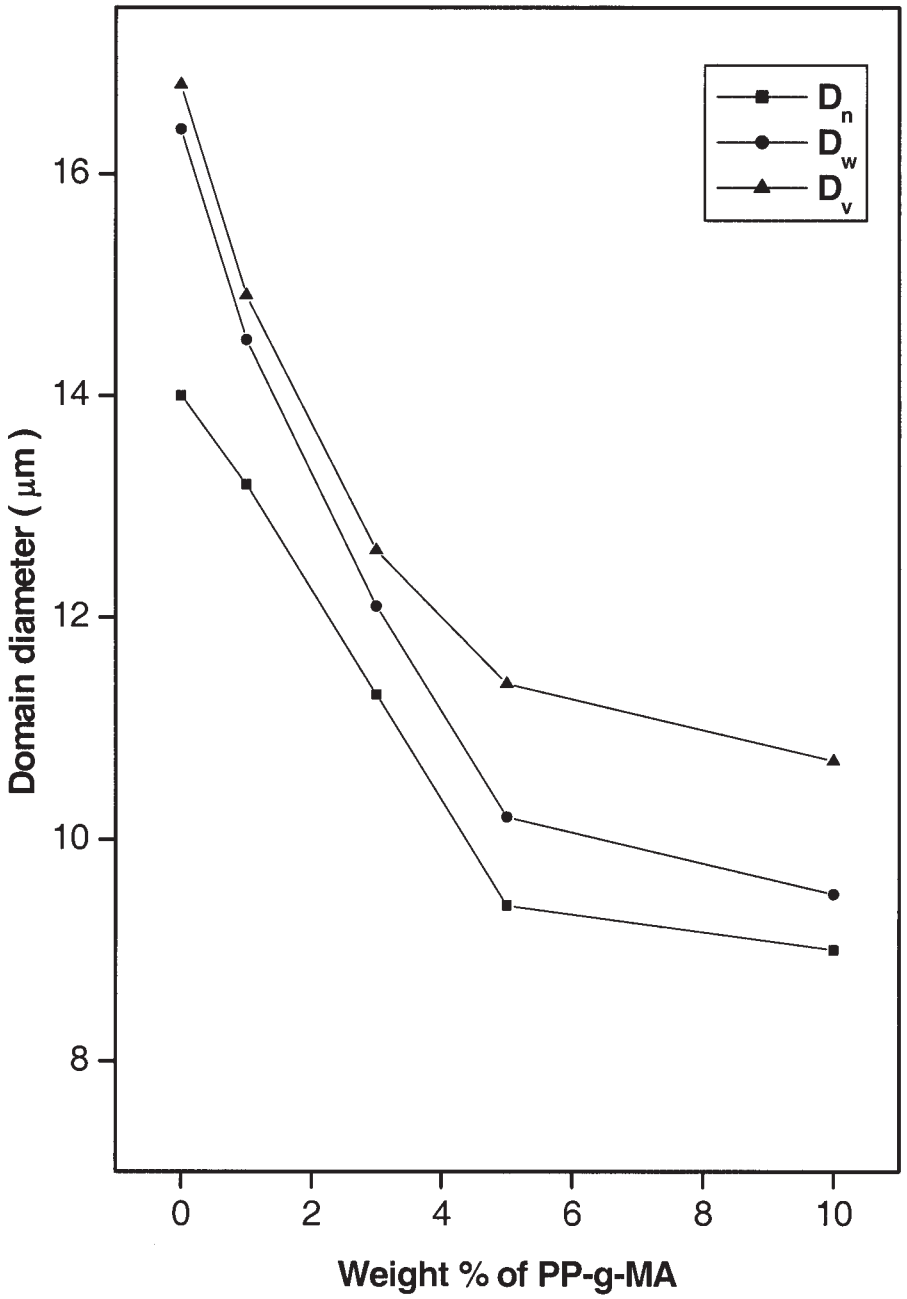

Figure 5 Effect of PP-g-MA concentration on the average domain size of dispersed PP phase in PAI2/PP 70/30 blends.

where λ is the ratio of the viscosities of the dispersed phase to that of the matrix phase, $C = 0.40$ is a numerical constant and R_{min} is the smaller particle radius between two particles. From this equation, it is clear that as λ increases h_0 increases. On the other hand, when the viscosity of the dispersed phase is greater than that of the matrix, the rate of coalescence will increase. This was found to hold for the present system also when PP dispersed particles were found to be larger than PA dispersed particles in the related blends, as mentioned earlier. It is obvious from Equation 13 that although the compatibiliser has noticeable effect, it is the viscosity ratio that plays the main role as far as this step is concerned.

The second stage of coalescence process is the drainage of the matrix trapped between the particles until the film thickness reaches its critical value, h_c.

$$h_c = (AR/8\pi\Gamma)^{1/3} \tag{14}$$

where A is the Hamaker constant, which represents the van der Waals interactions between neighboring particles. Compatibilisers have profound impact on

this step of coalescence process. Usually, a compatibiliser locates at the interface between the particles. Increase in the interfacial thickness with simultaneous increase in the value of h_c consequently mean favorable interactions between the dispersed particles. The ultimate effect is a reduction in particle size. Thus, the presence of compatibiliser, formed by the chemical reactions displayed in Figure 1, decreases the average domain size of the dispersed PP phase in PA matrix. However, it is worth mentioning that at a particular concentration of the compatibiliser, the interface becomes saturated as mentioned earlier and the compatibiliser seems to be unable to decrease the rate of coalescence further. This is the reason why there is no significant reduction in particle size beyond 5 wt % addition of the compatibiliser. Third stage of coalescence is the rupture of film due to interfacial instability and the final step is the merging of the particles. These two steps mainly depend on the second step and, therefore, compatibilisers have indirect effect on these two steps.

It is obvious from Table III that the polydispersity of dispersed particles reduces from 1.18 to 1.05. This is a clear indication of action of compatibiliser, which makes the phase morphology more uniform and stable by diminishing the chances of agglomeration of dispersed particles. A similar observation is obtained from Figure 6, which presents the influence of addition of PP-g-MA on the domain size distribution of PA12/PP = 70/30 blends. It can be seen that the domain size distribution becomes narrower by increasing concentration of PP-g-MA. The interfacial area per unit volume, on the other hand, increases monotonically in the presence of compatibiliser. As aforementioned, the interfacial chemical reaction between PP-g-MA and PA phase broadens the interface between PP and PA. Finally, it is evident from the table that IPDC comes down from 2.82 to 1.91 μm in presence of 5 wt % compatibiliser. Further, it is not significantly affected even by doubling the compatibiliser concentration.

In short, in terms of all morphological parameters summarized in Table III, it is clear that compatibiliser makes the phase morphology more fine, uniform, and stable, and it is important to note that beyond 5 wt % concentration of the compatibiliser, there is no notable change in any morphological parameters. Thus, for 70/30 PA12/PP blends, 5 wt % addition of PP-g-MA compatibiliser is sufficient for interfacial saturation.

Leibler[47] examined the emulsifying effect of an A-B copolymer in immiscible blend of polymers A and B and predicted a reduction of interfacial tension caused by equilibrium adsorption of the copolymer at the interface. He suggested that at equilibrium, the droplets' size distribution is controlled by rigidity and spontaneous curvature of radius of the interphase, both dependent on the copolymer's molecular constitution. According to the author, the interfacial tension reduction is given by the relation:

$$\Delta\gamma = -(kT/a^2)(3/4)^{1/3}(\Sigma/\alpha^2)^{-5/3} \times (Z_{CA}Z_A^{-2/3} + Z_{CB}Z_B^{2/3}) \quad (15)$$

where Z_{CA} and Z_{CB} are the number of A and B units in the copolymer, respectively, Z_A and Z_B are the degree of polymerization of A and B, respectively, a is the monomer's unit length, Σ is the interfacial area per copolymer. According to Noolandi,[48] the effect of copolymer on surface tension between the two phases is mainly influenced by the contributions from a series of factors such as lowering of interaction energy between the immiscible homopolymers, the broadening of the interface between the homopolymers, the entropy reduction in the system, a decrease in energy of interaction of the two blocks with each other, and a large decrease in the interaction energy of the oriented blocks with homopolymers. However, it should be noted that the localization of copolymer at the interface and the separation of blocks into corresponding homopolymer phases and the simultaneous reduction in interfacial tension between the phases depend on various factors such as mixing conditions, interaction of the compatibiliser with the dispersed phase, molecular weight and composition of the compatibiliser, the rate of absorption, and orientation of the compatibiliser at the interface. Based on these facts and by neglecting the loss of conformational entropy, Noolandi[49] derived an equation for the interfacial tension reduction as:

$$\Delta\gamma = d\Phi_c[1/2\chi + 1/Z_c - 1/Z_c \exp(Z_c\chi/2)] \quad (16)$$

where d is the width at half height of the copolymer profile reduced by the Kuhn statistical segment length, Φ_c the bulk copolymer volume fraction of the copolymer in the system, Z_c is the degree of polymerization of the copolymer, and χ is the Flory–Huggins interaction parameter between A and B segments. As the interfacial tension reduction is directly proportional to the particle size reduction, Wu[42] argued that

$$\Delta D = Kd\Phi_c[1/2\chi + 1/Z_c \exp(Z_c\chi/2)] \quad (17)$$

where K is proportionality constant.

Figure 7 presents a plot of domain size reduction (ΔD) as a function of the volume fraction of PP-g-MA for 70/30 PA12/PP blends. This figure reveals that below a critical micelle concentration (CMC) ΔD decreases almost linearly with increasing concentration of PP-g-MA, whereas beyond CMC, a leveling off is observed, in agreement with the predictions of Noolandi and Hong.[49,50]

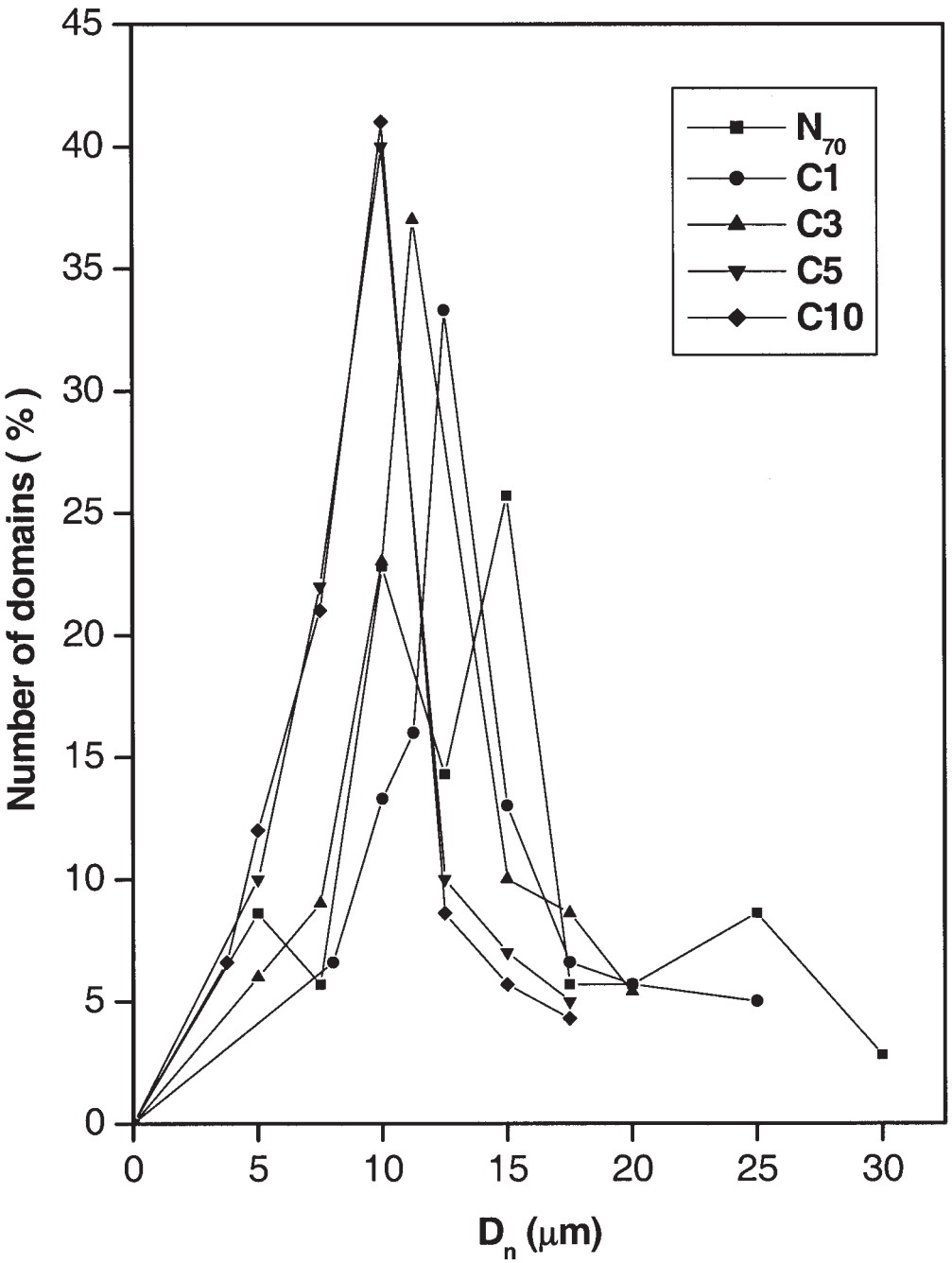

Figure 6 Effect of compatibilisation on the domain distribution of dispersed PP phase in PA12/PP 70/30 blends.

Tensile properties of PA12/PP blends

Tensile properties of the blends are depicted in Table IV. All the blends showed negative deviation because of the highly immiscible and incompatible nature of the components as evident from the morphological studies. Maximum tensile strength is shown by neat PA12. Addition of PP decreased the tensile strength of the blends and the minimum tensile strength is found for N_{60}, $N_{50,}$ and N_{40} blends. This may be due to the maximum unfavorable cross correlation due to highly immiscible and incompatible nature of these blends, as revealed from the morphological parameters.

Tensile strength at break (TS_b) and elongation at break (E_b) showed no regular trend. Addition of PP decreased the elongation at break of blends up to 50 wt % of PP. The blend that possessed maximum elongation at break was N_{10}. Regarding the Young's modulus, all the blends except N_{60}, $N_{50,}$ and N_{40} exhibited almost constant values. Since measured at low strain levels, Young's modulus does not depend considerably on the incompatibility between the components. However, a very high immiscibility may affect the Young's modulus of the blends. Further, the Young's modulus depends on the crystallinity changes during

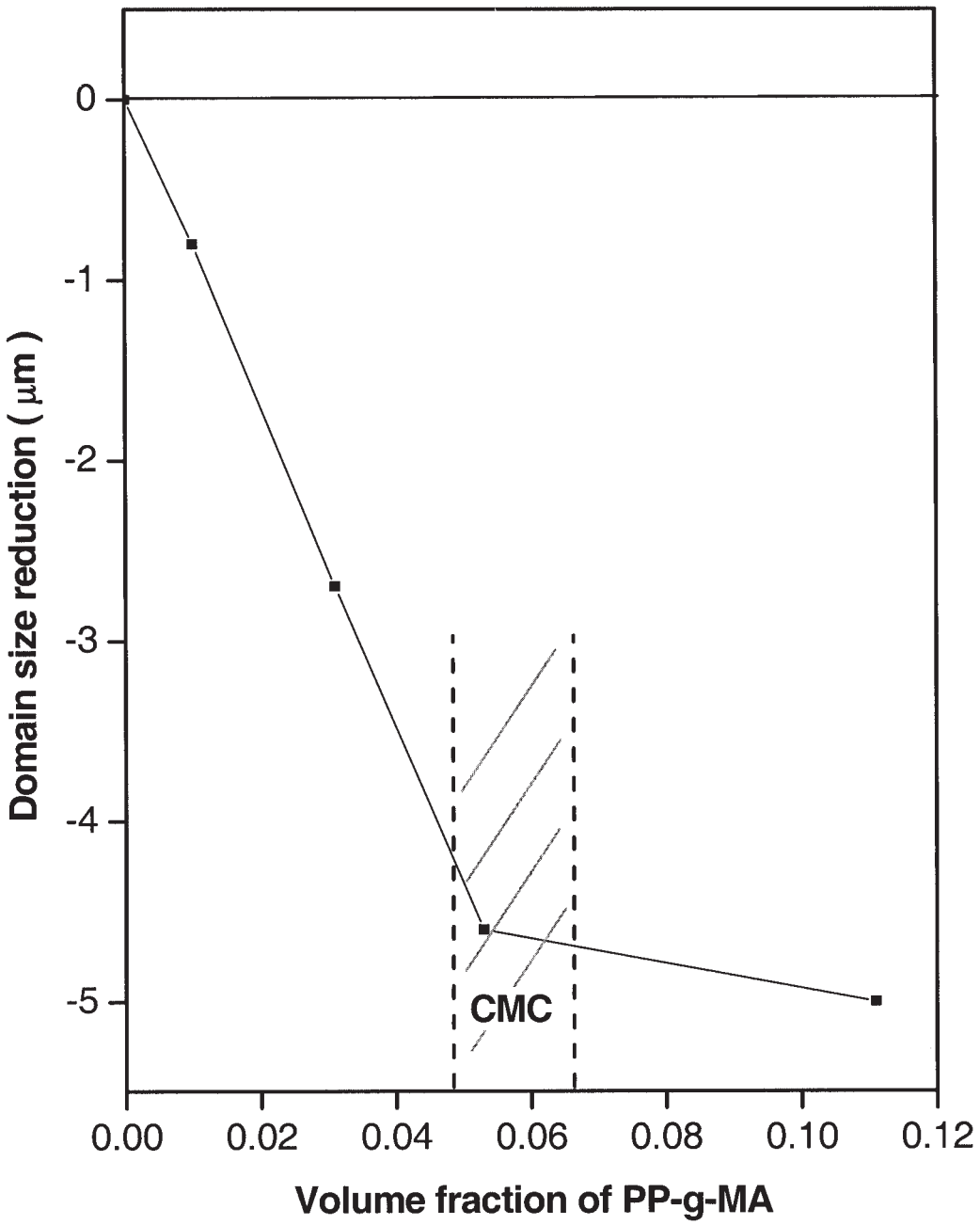

Figure 7 Effect of volume fraction of PP-g-MA on the domain size reduction of PA12/PP 70/30 blends.

blending. So, presence of PP in PA12 and PA12 in PP matrices may not have much effect on the Young's modulus of the blends in terms of incompatibility. For N_{60}, N_{50}, and N_{40} blends, both the incompatibility factor and crystallinity changes may be adversely affected and, therefore, these blends exhibited minimum values. Owing to the maximum incompatibility, the blends N_{60}, N_{50}, and N_{40} suffered maximum deterioration in tensile properties. This is in good agreement with the phase morphological observations.

Effect of compatibilisation on the tensile properties of the blends is summarized in Table V. Figure 8 displays the variation of tensile strength of 70/30 blends as a function PP-g-MA. It is noteworthy that the compatibiliser acts as interfacial emulsifying agent. Regarding the tensile strength, addition of PP-g-MA increased the tensile strength considerably, and the maximum value for tensile strength was found for the blend containing 10 wt % compatibiliser. Here, an 85% increase of tensile strength was noticed. The reason for the increase in tensile strength by the addition of compatibiliser is clear. As mentioned earlier, the nature of interface has a crucial role in determining the bulk properties of

TABLE IV
Tensile Properties of PA12/PP Uncompatibilised Blends

Designation	Composition of PA12/PP	Maximum tensile strength (MPa)	Tensile strength at break (MPa)	Elongation at break (%)	Young's modulus (MPa)
N_{100}	100/0	47.0 ± 1.4	29.0 ± 0.9	75 ± 4	1550 ± 40
N_{90}	90/10	40.3 ± 1.1	16.8 ± 0.7	23 ± 2	1530 ± 50
N_{80}	80/20	31.7 ± 0.9	29.1 ± 0.8	20 ± 2	1410 ± 30
N_{70}	70/30	23.9 ± 0.7	23.5 ± 0.7	18 ± 2	1540 ± 60
N_{60}	60/40	17.7 ± 0.6	17.6 ± 0.5	14 ± 1	955 ± 40
N_{50}	50/50	16.1 ± 0.5	15.9 ± 0.6	15 ± 1	1310 ± 40
N_{40}	40/60	18.7 ± 0.6	15.9 ± 0.7	16 ± 1	1070 ± 40
N_{30}	30/70	20.1 ± 0.7	18.9 ± 0.7	23 ± 2	1740 ± 70
N_{20}	20/80	25.4 ± 0.8	19.7 ± 0.6	20 ± 2	1660 ± 50
N_{10}	10/90	31.3 ± 0.9	20.0 ± 0.5	47 ± 3	1740 ± 60
N_0	0/100	35.0 ± 1.1	27.0 ± 0.8	27 ± 2	1660 ± 60

multiphase systems. Compatibiliser formed as a result of interfacial chemical reaction, locates at the interface between the polymers in the blend and diminishes unfavorable interactions between the components and enhances favorable interactions at the interfaces and thereby: (a) improves the interfacial adhesion between the components in the blends, (b) reduces the interfacial tension, (c) regulates the rate of coalescence, and (d) stabilizes the phase morphology of the blends.

These were already evident from morphological studies which revealed that presence of compatibiliser decreased the particle size and made the phase morphology more fine, uniform, and stable. The morphological parameters derived inform us that compatibiliser improved the interfacial properties (such as interface thickness, strength, and surface area). However, it is interesting to note that based on morphological parameters it is found that 5 wt % compatibiliser is sufficient to saturate the interface, and evaluation of tensile strength showed that maximum tensile strength was observed at 10 wt % concentration of compatibiliser. These results offer an apparent conflict with the phase morphological results. However, this may be due to some reinforcing effect of excess compatibiliser after saturating the interface. There is, however, still some uncertainty and a detailed investigation is needed.

The tensile strength at break values are found to be increased on compatibilisation, even though elongation at break did not change as a function of compatibiliser concentration. It is also interesting to notice that the Young's moduli were not appreciably affected. This also reveals that compatibility has no considerable effect on the stiffness properties, which are determined at relatively low strain levels.

Theoretical modeling

Theoretical analysis of tensile strength

To understand the level of interaction between the component polymers in PA12/PP blends, predictive models were used to tensile strength data. These models include:

i. Nielsen's first power law model[51]

$$\frac{\sigma_b}{\sigma_p} = (1 - \phi_1)S \tag{18}$$

ii. Nielsen's two-third power law model[51]

$$\frac{\sigma_b}{\sigma_p} = (1 - \phi_1^{2/3})S' \tag{19}$$

iii. Nicolais–Narkis model[52]

TABLE V
Effect of Compatibilisation on the Tensile Properties of PA12/PP Blends

Designation	Maximum tensile strength (MPa)	Tensile strength at break (MPa)	Elongation at break (%)	Young's modulus (MPa)
N_{70}	23.9 ± 0.7	23.5 ± 0.7	18 ± 2	1540 ± 60
C_1	26.2 ± 0.8	24.4 ± 0.6	22 ± 2	1460 ± 50
C_3	36.0 ± 1.0	34.0 ± 0.8	18 ± 2	1560 ± 50
C_5	38.6 ± 1.2	37.0 ± 0.8	18 ± 2	1540 ± 40
C_{10}	44.2 ± 1.3	44.2 ± 0.9	16 ± 2	1690 ± 60

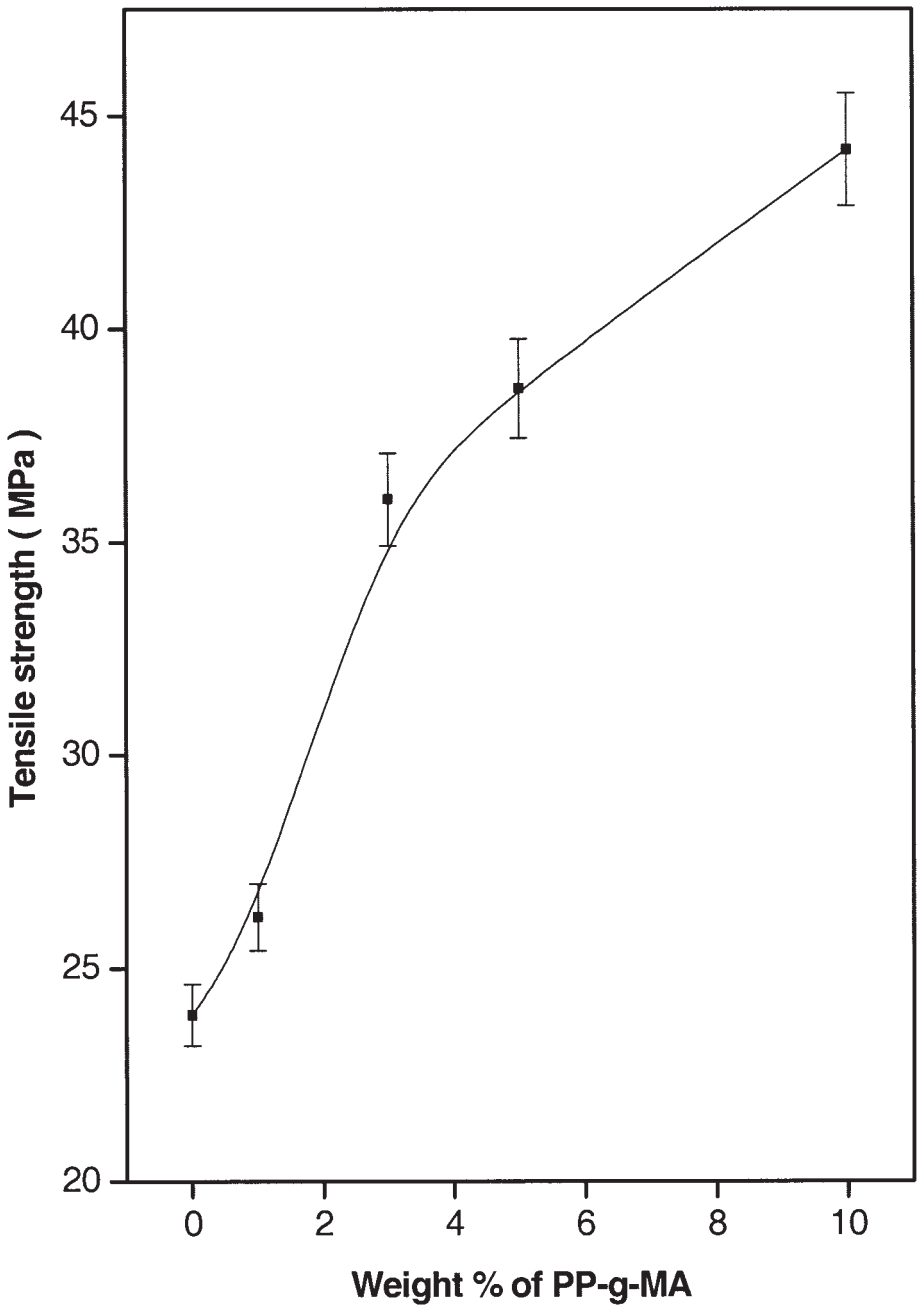

Figure 8 Effect of concentration of PP-g-MA on the tensile strength of PA12/PP 70/30 Blends.

$$\frac{\sigma_b}{\sigma_p} = (1 - K_b\phi_1^{2/3}) \tag{20}$$

where σ_b and σ_p represent the tensile strength of the blend and the major component of the blend respectively, ϕ_1 is the volume fraction of the minor phase, S and S' are Nielsen's parameters in the first and two-third power law models, respectively, and K_b is an adhesion parameter. S and S' account for the weakness in the structure brought about by the discontinuity in stress transfer and generation of the stress concentration at the interfaces in the case of blends. The value of S and S' are unity in the case of no stress concentration effect. The value of K_b is 1.21 for spherical inclusions of the minor phase having no adhesions. The values of relative tensile strength (σ_b/σ_p), S, S', and K_b are listed in Table VI. Plots of relative tensile strength versus volume fraction of the blends predicted using the three models are presented in Figures 9–14.

A plot of relative tensile strength values predicted from Nielsen's first power law model with $S = 1$, $S = 0.80$ and experimental results plotted against the volume fraction of PP phase is given in Figure 9. The line

TABLE VI
Values of Stress Concentration Parameters in PA12/PP Blends with PP Dispersed Phase

Designation	σ_b/σ_p	S	S'	K_b
N_{90}	0.895	0.995	1.140	0.488
N_{80}	0.704	0.880	1.070	0.870
N_{70}	0.530	0.757	0.958	1.050
N_{60}	0.393	0.655	0.860	1.170
N_{50}	0.358	0.716	0.967	1.020
Mean	0.576	0.801	0.999	0.919

with $S = 1$ represents perfect adhesion. It has been found that the experimental results are closer to this line only in the beginning, i.e., blend containing only 10 wt % of PP. Beyond 10 wt % PP, the experimental results are more close to the line with $S = 0.8$ up to 30 wt % and there after moves away from the line for 40 wt % PP and toward the end (50 wt % of PP) it again comes closer to the line with $S = 0.80$. This is in close agreement with the morphological parameters. As the concentration of dispersed PP phase increases, the incompatibility increases as a result of the fact that the

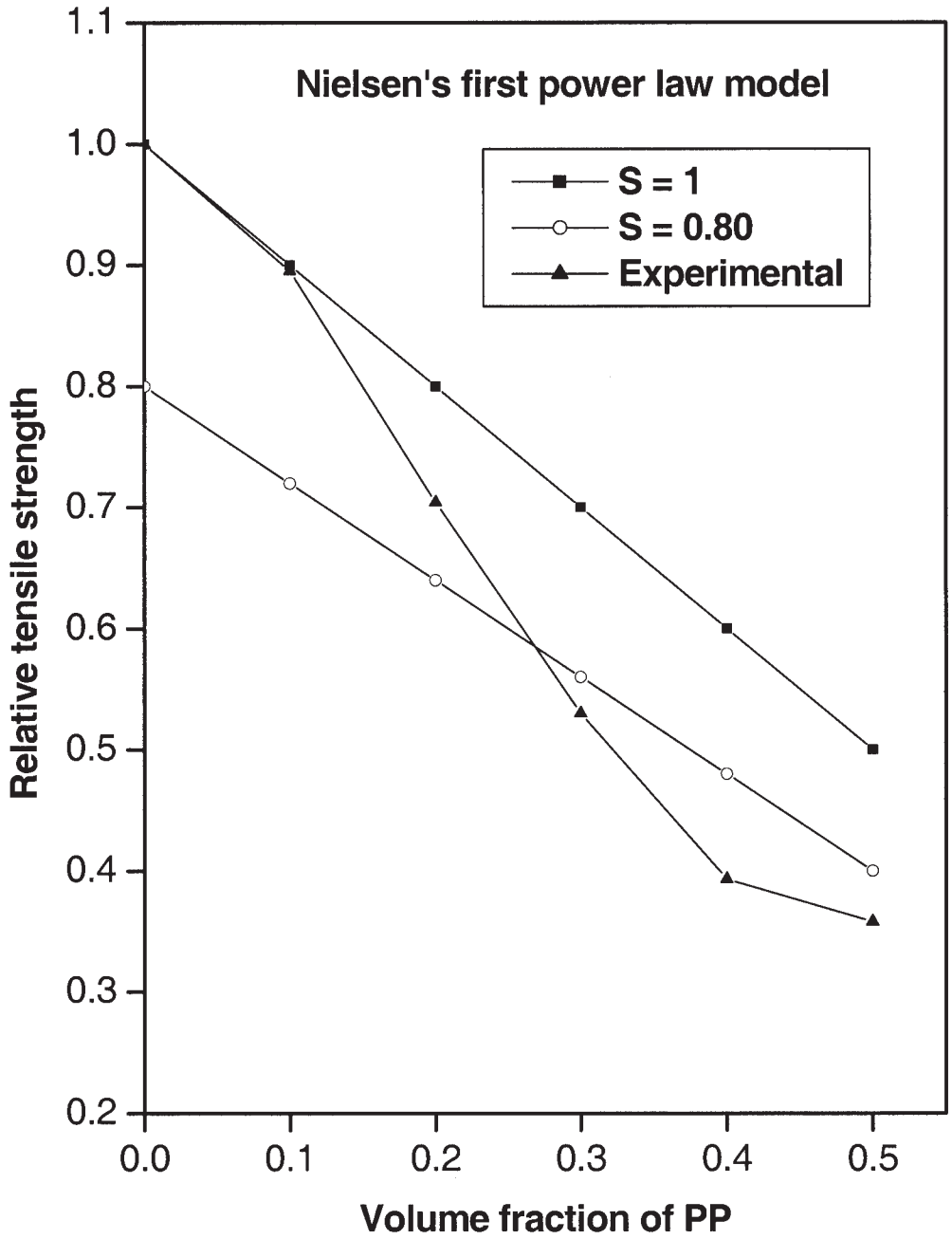

Figure 9 Plot of relative tensile strength versus volume fraction of dispersed PP phase, using Nielsen's first power law model.

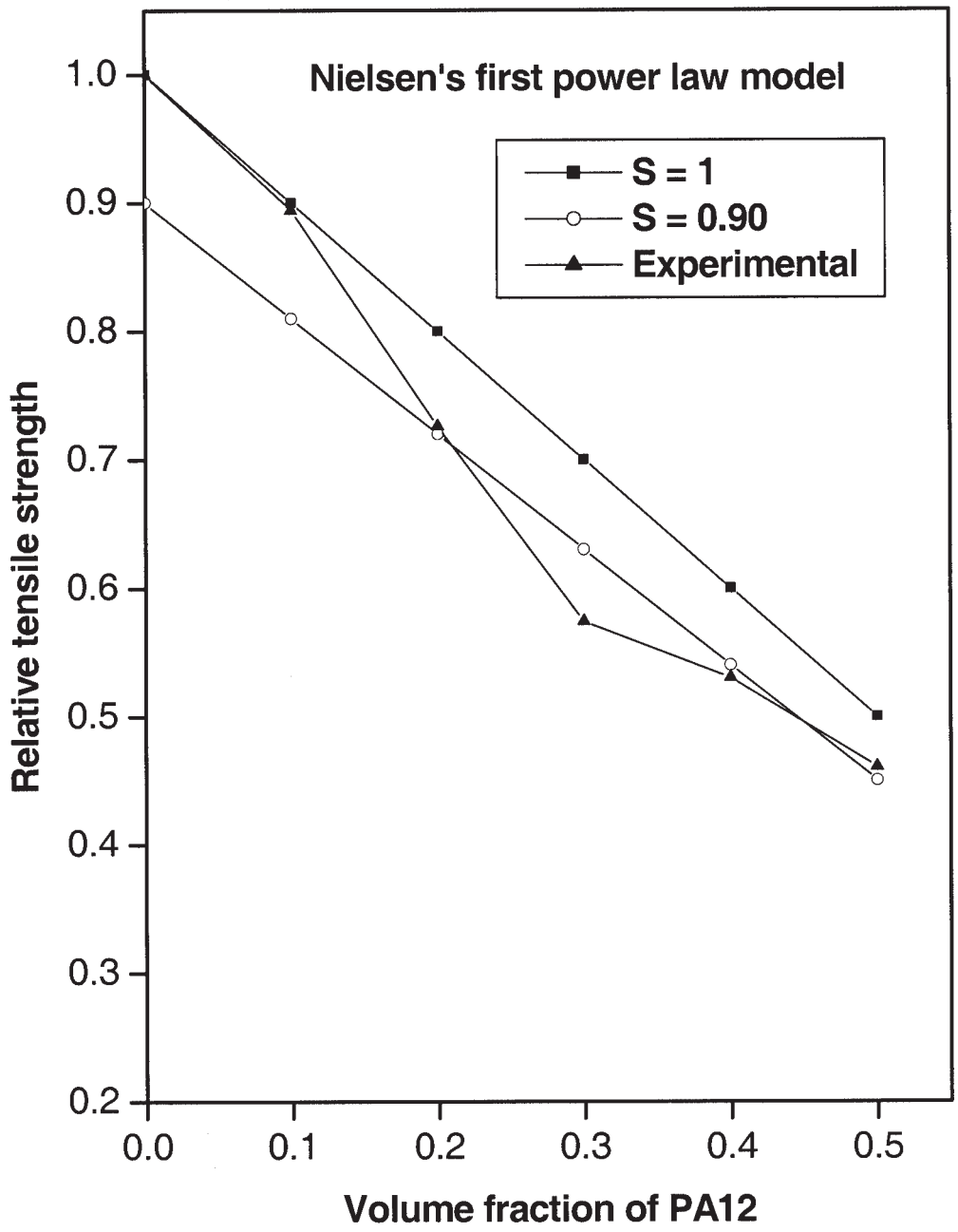

Figure 10 Plot of relative tensile strength versus volume fraction of dispersed PA12 phase, using Nielsen's first power law model.

morphology becomes unstable. This means that beyond 10 wt % of PP, the blend is converted from a no-stress concentration system to a structure with significant stress concentration around PP. In other words, this behavior shows that beyond 10 wt % of PP concentration, the blends fail to take excessive stress because of poor interfacial adhesion. Plot of relative tensile strength predicted from Nielsen's first power law model with $S = 1$, $S = 0.90$, and experimental results plotted against the volume fraction of PA12 dispersed phase is presented in Figure 10. It is obvious from the figure that blend with 10 wt % dispersed PA12 in PP is in perfect agreement with the theoretical line indicating perfect adhesion. However, beyond this, the experimental results deviate from the theoretically predicted line. However, it should be noted that for 40 wt % and 50 wt % concentration of PA, the experimental results are in agreement with line with $S = 0.90$. Here also, it can be concluded that because of decrease in interfacial adhesion, beyond 10 wt % of PA12, the blend fails to take excessive stress. These facts are in perfect agreement with the morphological parameters as well as tensile properties.

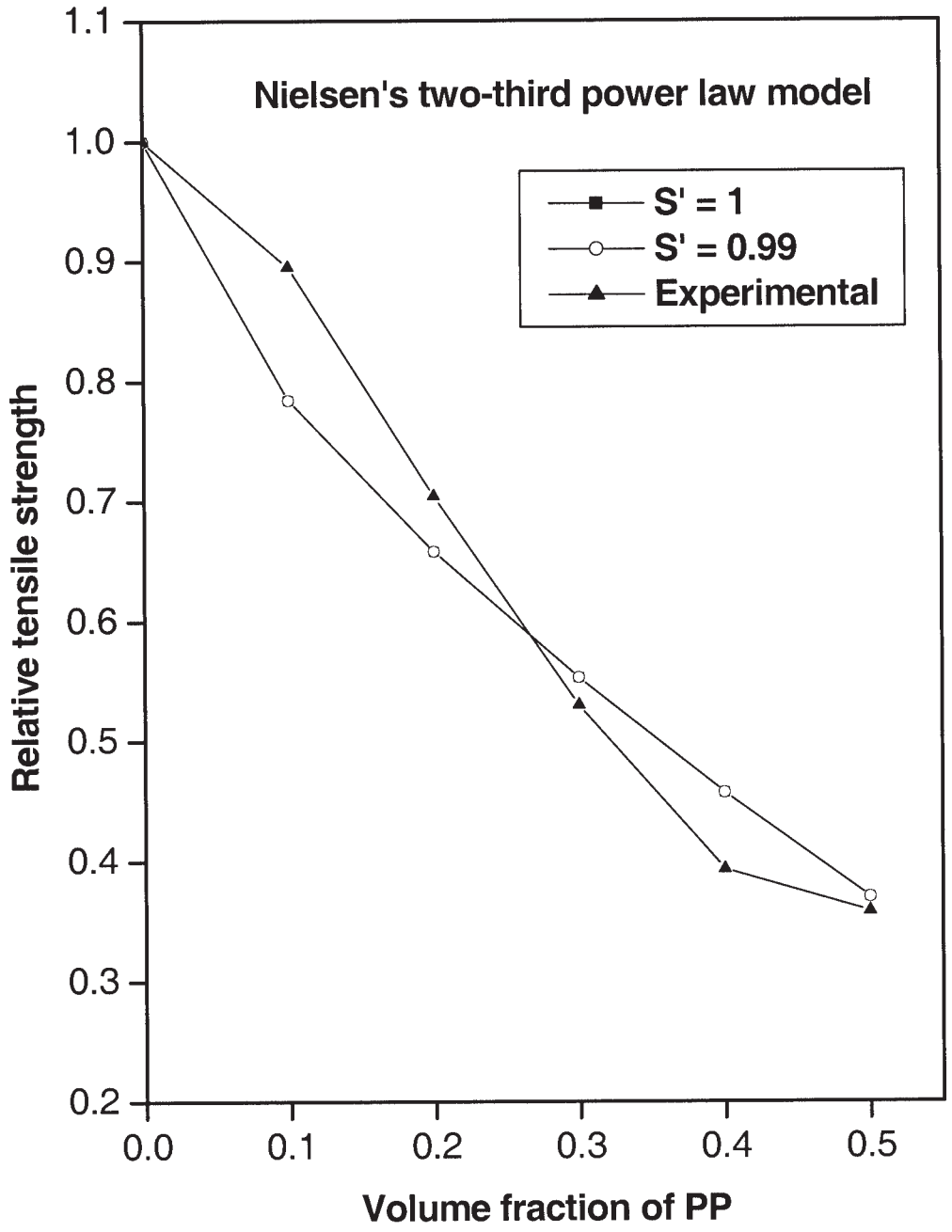

Figure 11 Plot of relative tensile strength versus volume fraction of dispersed PP phase, using Nielsen's two-third power law model.

Figure 11, presents the relative tensile strength values predicted from Nielsen's two-third power law model with $S' = 1$ and $S' = 0.99$ and experimental results as a function of volume fraction of PP. It should be noted that all the blends except N_{70} and N_{50} deviate from the theoretical values. However, note that the behavior obtained from this model is not in accordance with the experimental results of tensile strength. In Figure 12, the relative tensile strength values predicted from two-third power law model with $S' = 1$, $S' = 1.14$ and experimental results are plotted versus volume fraction of dispersed PA12 phase. It is observed that experimental results are in agreement with the theoretical results only for blend containing 30 wt % of PA12. However, this is not true as far as the tensile strength values are concerned. In short, Nielsen's two-third power law model is not best suited for the present system.

As mentioned earlier, the factor K_b, which is an adhesion parameter in Nicolais–Narkis model, has maximum value 1.21 if there is no adhesion. In

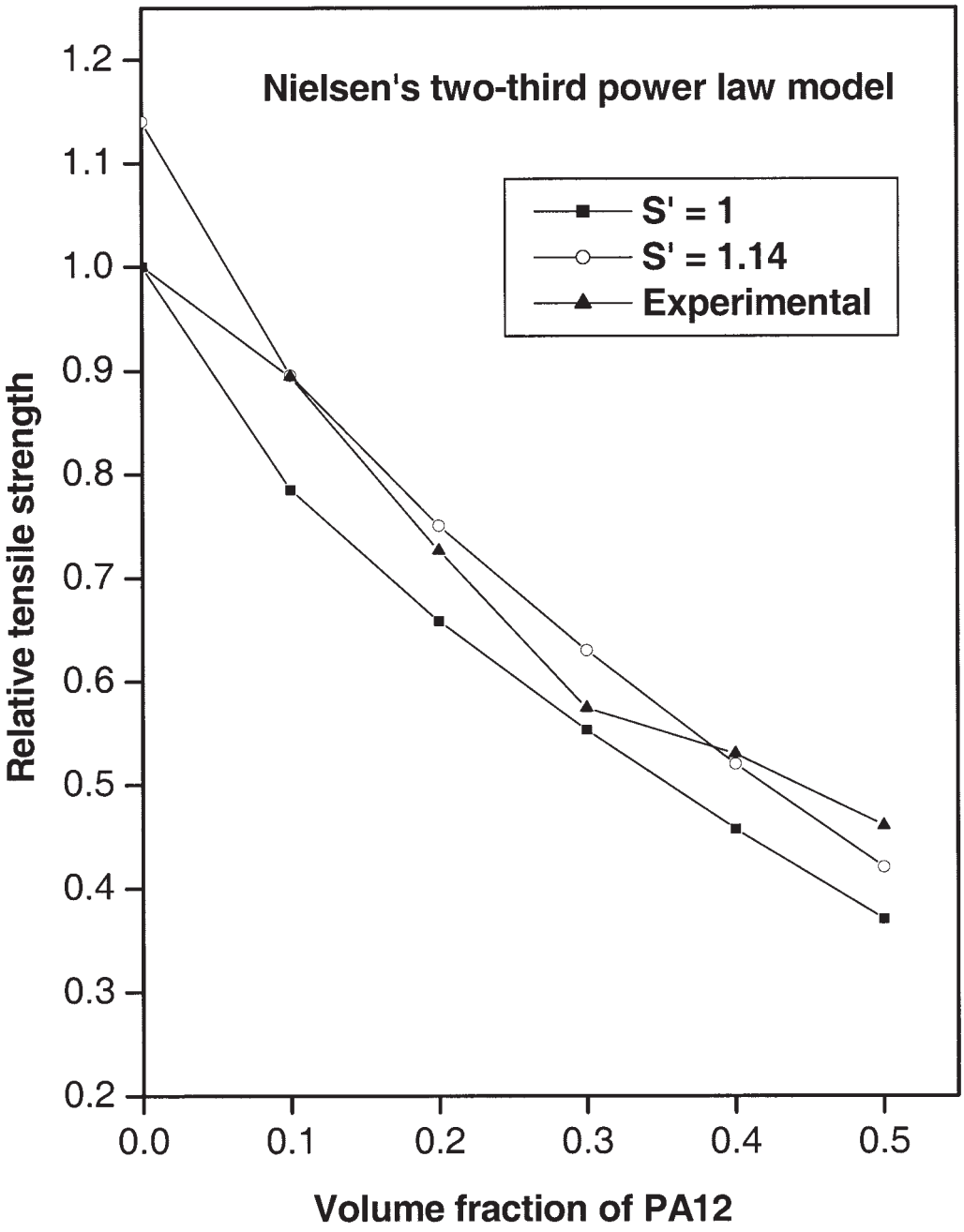

Figure 12 Plot of relative tensile strength versus volume fraction of dispersed PA12 phase, using Nielsen's two-third power law model.

Figure 13, the relative tensile strength values predicted with $K_b = 1.21$ and $K_b = 0.92$ and experimental results are plotted against the volume fraction of PP. The experimental values are away from those predicted from theory and even though small, the only blend that exhibits agreement with theory is N_{60}. However, the most important fact is that the experimental values lie above the theoretical curve. This means that there is no adhesion between the phases in the blend. Similarly, Figure 14, which is a plot of relative tensile strength values predicted from the same model with $K_b = 1.21$, $K_b = 0.80$ and experimental results versus volume fraction of PA12, also indicates the fact that the blends are incompatible and there is only very poor interfacial adhesion between the phases in the blend. In short, among the various predictive models that were used to analyze the tensile strength data of PA12/PP blends to assess the level of interfacial adhesion, Nielsen's first power law model was found to be best suited in terms of tensile properties as well as morphological parameters.

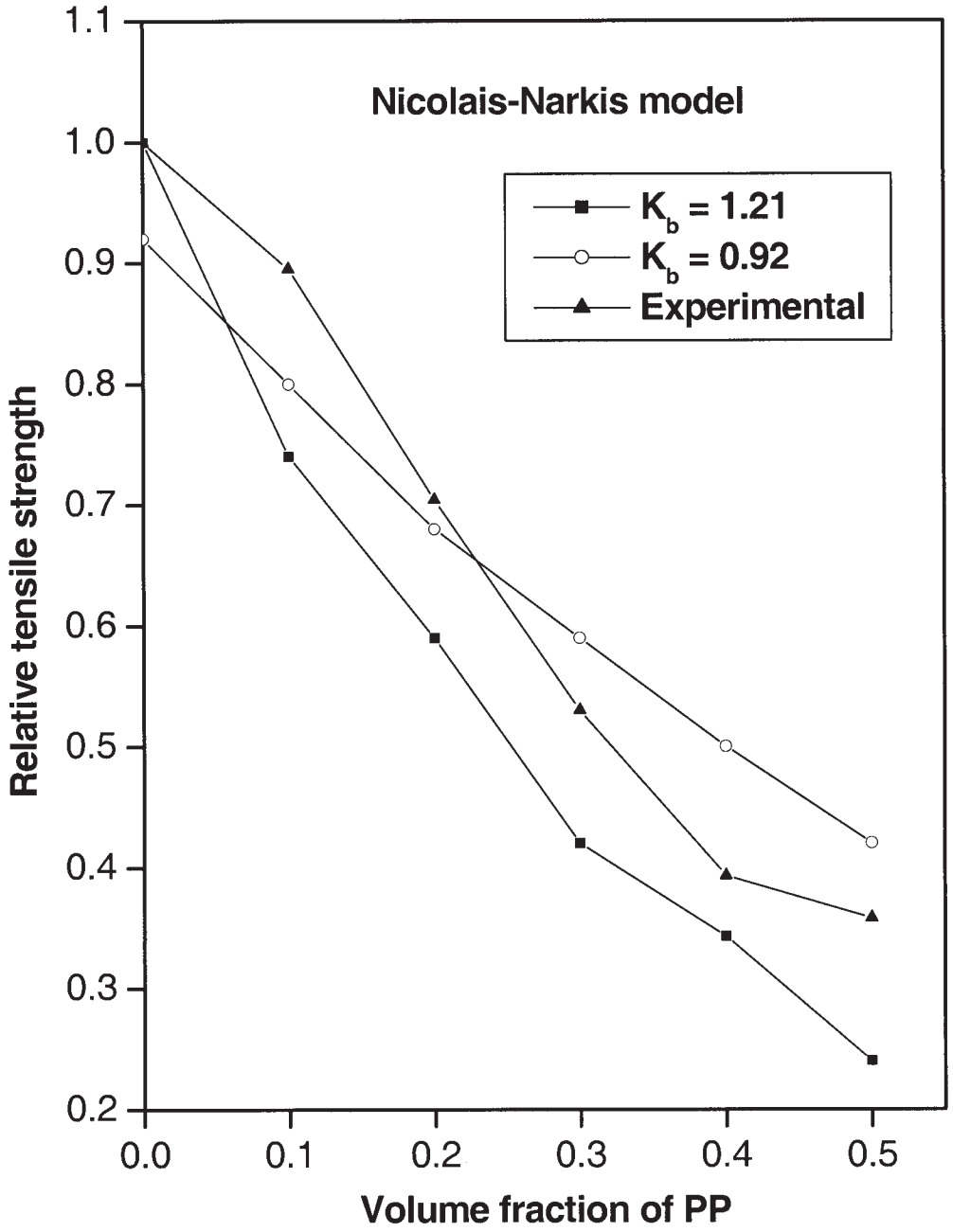

Figure 13 Plot of relative tensile strength versus volume fraction of dispersed PP phase, using Nicolais–Narkis model.

CONCLUSIONS

From the present study, which is devoted to investigate the effect of reactive compatibilisation on the phase morphology and mechanical properties of PA12/PP blends, the following conclusions can be drawn:

1. Phase morphology of uncompatibilized blends and the morphological parameters such as average domain size, poly dispersity (D_w/D_n), interfacial area (A_i), and critical inter particle distance (IPDC) revealed that PA12/PP blends exhibit an unstable and nonuniform phase morphology owing to the incompatible nature of the blend.
2. Presence of compatibiliser made the phase morphology more fine, uniform, and stable by diminishing the coalescence process and thereby improving the interfacial properties, and 5 wt % compatibiliser is sufficient to saturate the interface.
3. Tensile properties of uncompatibilized blends showed negative deviation due to the incompat-

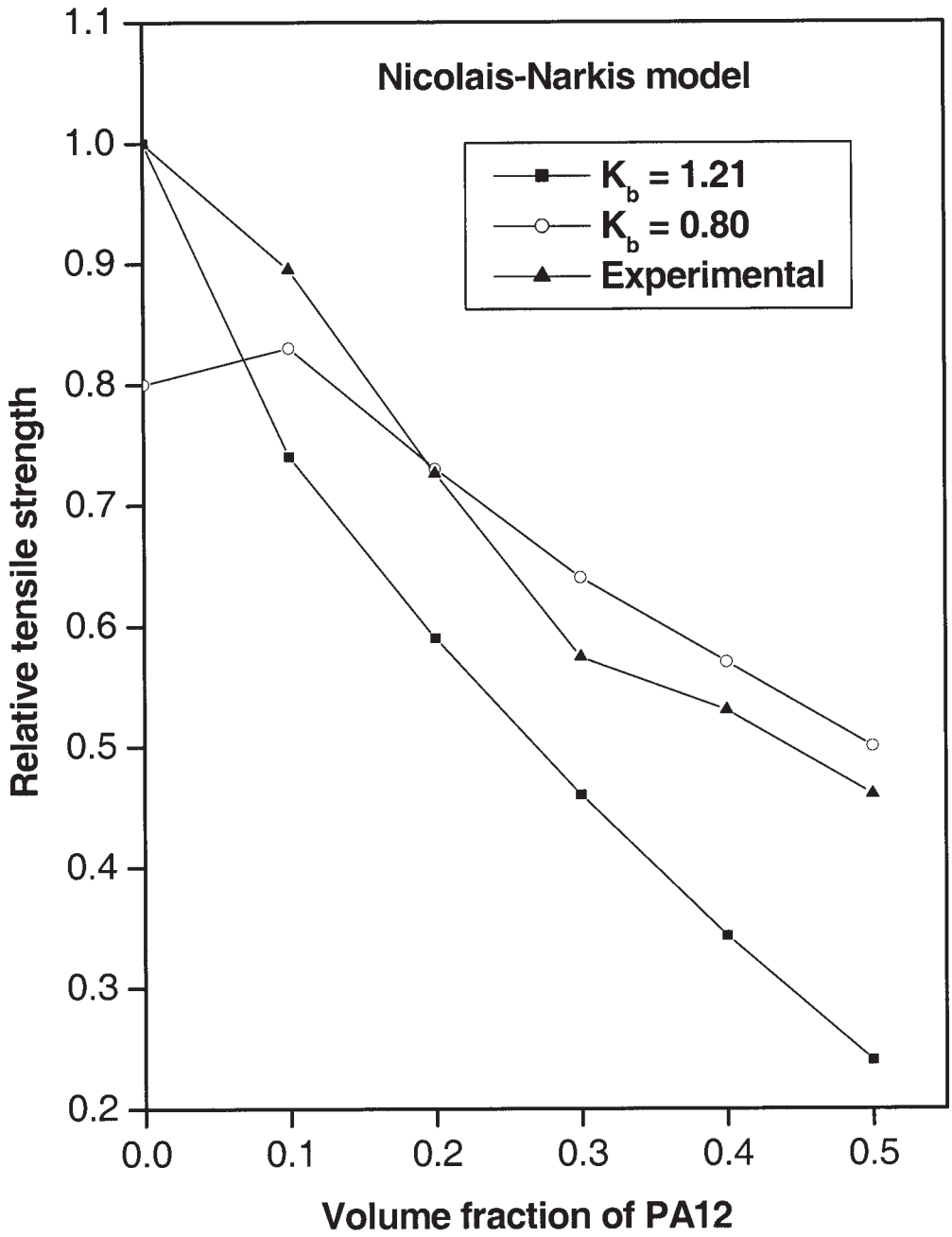

Figure 14 Plot of relative tensile strength versus volume fraction of dispersed PAI2 phase, using Nicolais–Narkis model.

ible nature of the blends and because of the maximum incompatibility N_{40}, N_{50}, and N_{60} blends exhibited maximum deterioration in tensile strength.

4. Presence of compatibiliser improved the tensile strength considerably. In contrary to the morphological observations, blends with 10 wt % compatibiliser exhibited maximum improvement in tensile strength.
5. Among the three models (Nielsen's first power law model, Nielsen's two-third power law model and Nicolais–Narkis model) applied to analyze the tensile strength data of the blends to assess the level of interfacial interaction, Nielsen's first power law model was found to be the best suited with the experimental data.

References

1. Xanthos, M.; Dagli, S. S. Polym Eng Sci 1991, 31, 929.
2. Liu, N. C.; Baker, W. E. Adv Polym Technol 1992, 11, 249.
3. Groeninckx, G.; Sarkissiva, M.; Thomas, S. In Polymer Blends: Formulation and Performance; Wiley: New York, 2000; Chapter 14, p 417.
4. Majumdar, B.; Paul, D. R. In Polymer Blends; Paul, D. R.; Bucknall, C. B., Eds.; Wiley: New York, 2000; Vol. 1, Chapter 17, p 539.

5. Groeninckx, G.; Harrats, C.; Thomas, S. In Reactive Polymer Blending; Baker, W. E.; Scott, C.; Hua, G. H., Eds.; Hanser Publishers: Munich, 2001; Chapter 3, p 43.
6. Sunderaraj, U.; Macosko, C. W. Macromolecules 1995, 28, 2647.
7. Macosko, C. W.; Guegan, P.; Khandpur, A. K.; Nakayama, A.; Marechal, P.; Inoue, T. Macromolecules 1996, 29, 5590.
8. Lee, M. S.; Lodge, T. P.; Macosko, C. W. J Polym Sci Part B: Polym Phys 1997, 35, 2835.
9. Mekhilef, N.; Favis, B. D.; Carreau, P. J. J Polym Sci Part B: Polym Phys 1997, 35, 293.
10. Hlavatá, D.; Horák, Z.; Hromádková, J.; Lednický, F.; Pleska, A. J Polym Sci Part B: Polym Phys 1999, 37, 1647.
11. Oshishi, H.; Ikehara, T.; Nishi, T. J Appl Polym Sci 2001, 80, 2347.
12. Harrats, C.; Fayt, R.; Jérôme, R. Polymer 2002, 43, 863.
13. George, J.; Joseph, J. R.; Varughese, K. T.; Thomas, S. J Appl Polym Sci 1995, 57, 449.
14. Lepers, J. C.; Favis, B. D.; Tabar, R. J. J Polym Sci Part B: Polym Phys 1997, 35, 2271.
15. Vocke, C.; Anttila, U.; Heino, M.; Hietaoja, P.; Seppälä, J. J Appl Polym Sci 1998, 70, 1923.
16. Lacasse, C.; Favis, B. D. Adv Polym Technol 1999, 18, 255.
17. Thomas, S.; Groeninckx, G. Polymer 1999, 40, 5799.
18. Carone, E., Jr.; Kopcak, U.; Gonçalves, M. C.; Nunes, S. P. Polymer 2000, 41, 5929.
19. Bae, T. Y.; Park, K. Y.; Kim, D. H.; Suh, K. D. J Appl Polym Sci 2001, 81, 1056.
20. Oderkerk, J.; Groeninckx, G. Polymer 2002, 43, 2219.
21. Sathe, S. N.; Rao, G. S. S.; Rao, K. V.; Devi, S. Polym Eng Sci 1996, 36, 2443.
22. Yu, Z. Z.; Lei, M.; Ou, Y. C.; Hu, G. H. J Polym Sci Part B: Polym Phys 1999, 37, 2664.
23. Jeziòrska, R. Macromol Symp 2000, 170, 21.
24. Shieh, Y. T.; Liao, T. N.; Chang, F. C. J Appl Polym Sci 2001, 79, 2272.
25. Chen, G.; Dong, W.; Liu, J. J Appl Polym Sci 2001, 81, 782.
26. Patel, A. C.; Brahmbhatt, R. B.; Sarawade, B. D.; Devi, S. J Appl Polym Sci 2001, 81, 1731.
27. Marco, C.; Ellis, G.; Gómez, M. A.; Fatou, J. G.; Arribas, J. M.; Campoy, I.; Fontecha, A. J Appl Polym Sci 1997, 65, 2665.
28. Turati, E.; Vitale, A.; Gallazzi, M.; Seves, A.; Testa, G. Adv Polym Technol 1998, 17, 317.
29. Covas, J. A.; Machado, A. V.; Duin, M. V. Adv Polym Technol 2000, 19, 260.
30. George, J.; Ramamurthy, K.; Varughese, K. T.; Thomas, S. J Polym Sci Part B: Polym Phys 2000, 38, 1104.
31. George, S.; Nelakantan, N. R.; Varughese, K. T.; Thomas, S. J Polym Sci Part B: Polym Phys 1997, 35, 2309.
32. Citterio, C.; Selli, E.; Testa, G.; Bonfatti, A. M.; Seves, A. Angew Makromol Chem 1999, 270, 22.
33. Pesneau, I.; Cassagnau, P.; Michel, A. J Appl Polym Sci 2001, 82, 3568.
34. Roover, B. D.; Devaux, J.; Legras, R. J Polym Sci Part A: Polym Chem 1997, 35, 901.
35. Nielsen, L. E. Rheol Acta 1974, 13, 86.
36. Danesi, S.; Porter, R. S. Polymer 1978, 19, 448.
37. Paul, D. R.; Barlow, J. W. J Macromol Sci Rev Macromol Chem 1980, 18, 109.
38. Han, C. D. Multiphase Flowing in Polymer Processing; Academic Press: New York, 1982.
39. Roland, C. M.; Boühm, G. G. A. J Polym Sci Part B: Polym Phys 1984, 22, 79.
40. Elmendrop, J. J.; Maalche, R. J Polym Eng Sci 1985, 25, 1041.
41. Taylor, G. I. Proc R Soc London Ser A 1934, 146, 501.
42. Wu, S. Polym Eng Sci 1987, 27, 342.
43. Van Oene, H. J Colloid Interface Sci 1972, 40, 448.
44. Tokita, N. Rubber Chem Technol 1977, 50, 292.
45. Wu, S. Polymer 1985, 26, 1855.
46. Yu, W.; Zhou, C.; Inoue, T. J Polym Sci Part B: Polym Phys 2000, 38, 2378.
47. Leibler, L. Makromol Chem Macromol Symp 1988, 16, 1.
48. Noolandi, J. Polym Eng Sci 1984, 24, 74.
49. Noolandi, J.; Hong, K. M. Macromolecules 1982, 15, 482.
50. Noolandi, J.; Hong, K. M. Macromolecules 1984, 17, 1531.
51. Nielsen, L. E. J Appl Polym Sci 1966, 10, 97.
52. Nicolais, L.; Narkis, M. Polym Eng Sci 1971, 11, 194.